NJC

PAPER

View Article Online
View Journal

Cite this: DOI: 10.1039/c8nj03272f

Fried egg-like Au mesostructures grown on poly(4-vinylpyridine) brushes grafted onto graphene oxide†

Lihua Feng,[a] Ke Wang,[a] Ping Li,[a] Wenqin Wang *[a] and Tao Chen *[b]

Received 1st July 2018,
Accepted 9th September 2018

DOI: 10.1039/c8nj03272f

rsc.li/njc

The controlled growth of noble metal micro/nanostructures on graphene films is of crucial importance for high-quality surface-enhanced Raman scattering (SERS) spectra. In this paper, we described the *in situ* fabrication of different Au structures on poly(4-vinylpyridine) (P4VP) brush-grafted graphene oxide (GO). The proposed strategy is based on the use of $HAuCl_4$-loaded P4VP brushes grown on GO as a reaction chamber. The novel Au mesostructures with a "fried egg-like" morphology were fabricated on the surface of the GO-P4VP films using ascorbic acid (AA) as a weaker reducing agent. The obtained GO-P4VP/fried egg-like Au composites can be used as substrates for surface-enhanced Raman scattering (SERS) and exhibited good SERS sensitivity for detecting 4-aminothiophenol (4-ATP) molecules.

1. Introduction

Surface enhanced Raman scattering (SERS), as an ultrasensitive and nondestructive analytical technique, has garnered ever-increasing scientific interest in chemical production, biochemistry and environmental monitoring.[1,2] Recently, graphene-based noble metal composites as SERS-active substrates have received considerable attention.[3] The attractive features of these composites are that besides the noble metal (especially Ag and Au) nanoparticles (NPs) with rough surfaces having high SERS enhancement *via* electromagnetic enhancement, graphene (such as graphene oxide (GO) and reduced graphene oxide (rGO)) itself also exhibits a Raman enhancing effect *via* the chemical mechanism (CM).[4] More importantly, the combination of noble metal NPs with graphene endows the composites with a higher Raman enhancement than graphene or the noble metal NPs alone.[5] However, because graphene-enhanced Raman scattering has a relatively lower enhancement factor (EF) value (less than 10 to as high as $\sim$100) dominated by CM,[6] to improve the SERS EF of graphene-based noble metal NP composites, controlling the size, morphology and surface topography of noble metal NPs is still of crucial importance.

To date, various graphene-based noble metal composites as SERS substrates have been reported.[3] Unfortunately, owing to the relatively limited amount of functional groups on graphene, directly fabricating hierarchical noble metal NPs with sharp edges, tips and nanoscale junctions on the graphene surface is still a challenge. To overcome the above drawbacks, the surface modification of graphene with polymer materials to control the growth of noble metal NPs on graphene is a promising strategy.[7,8] Of all surface-modifying strategies, grafting polymer brushes onto graphene is particularly attractive.[9] Besides polymer brushes acting as a matrix to immobilize metal NPs[10] or *in situ* prepare noble metal NPs[11] for SERS measurement, they can also be facilely grafted onto graphene *via* a one-step reaction under UV-irradiation at room temperature, that is, by self-initiated photografting and photopolymerization (SIPGP) technology.[12] In our previous work, we also demonstrated that Ag and Au nanostructures could be obtained on polymer brushes grafted onto GO, which could be used as SERS-active substrates and exhibited an excellent SERS performance.[13,14]

In this work, we describe the *in situ* fabrication of Au NPs on poly(4-vinylpyridine) (P4VP) brushes grafted onto GO. The synthetic strategy is shown in Scheme 1: the GO flakes were transferred onto NH_2-terminated silicon wafers to form a GO film. P4VP brushes were grafted onto the GO film *via* SIPGP. $AuCl_4^-$ ions were bound to the P4VP chains as counter ions of the protonated pyridine groups. Tiny Au NPs and "fried egg-like" Au mesostructures were obtained using $NaBH_4$ and AA as reducing agents, respectively. The application of the as-obtained fried egg-like Au mesostructures in SERS was investigated.

[a] School of Materials Science and Chemical Engineering, Ningbo University, Ningbo 315211, P. R. China. E-mail: wqwang@126.com
[b] Division of Polymer and Composite Materials, Ningbo Institute of Material Technology and Engineering, Chinese Academy of Science, Ningbo 315201, P. R. China. E-mail: tao.chen@nimte.ac.cn

† Electronic supplementary information (ESI) available. See DOI: 10.1039/c8nj03272f

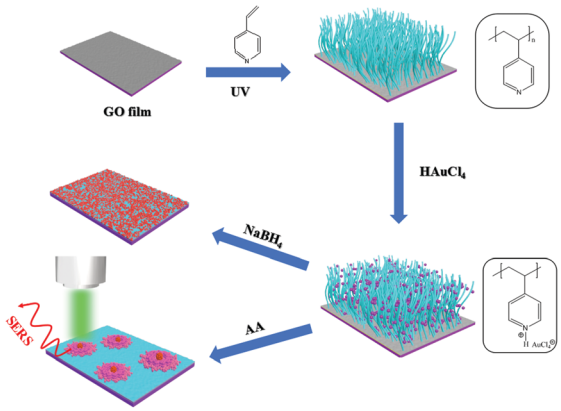

Scheme 1 Schematic procedure for the fabrication of P4VP brushes grafted onto GO sheets by SIPGP and the formation of Au NPs.

2. Experimental section

2.1 Materials

4-Vinylpyridine, 3-aminopropyltriethoxysilane (APTES) and 4-aminothiophenol (4-ATP) were purchased from Sigma-Aldrich. Pyrrole, $HAuCl_4 \cdot 4H_2O$ (99.8%), $NaBH_4$, ascorbic acid (AA), toluene, concentrated sulfuric acid, and H_2O_2 (30%) were obtained from Sinopharm Chemical Reagent Co. (Shanghai, China). 4-Vinylpyridine was distilled under reduced pressure before use. Other reagents were used as received without further purification. NH_2-terminated silicon wafers were obtained by surface modifying the silicon wafers with a 300 nm SiO_2 layer with 3-aminopropyltriethoxysilane (APTES) according to our previous reports.[13,14]

2.2 P4VP brushes grafted onto GO by SIPGP

The synthesis of GO flakes and transfer of GO onto NH_2-terminated silicon wafers were carried out according to the Hummers' method[15] and Chen's report,[16] respectively. The NH_2-terminated silicon wafer/GO films were put into a polymerization tube containing degassed 4-vinylpyridine monomer and irradiated with UV light (λ_{max} = 350 nm) at room temperature. SIPGP was allowed to proceed for 6 h. Subsequently, the as-obtained GO-P4VP films were cleaned by ultrasonication for 10 min in tetrahydrofuran and ethanol, respectively.

2.3 Synthesis of Au nanostructures on GO-P4VP film

The GO-P4VP films were immersed in a $HAuCl_4$ aqueous solution (0.01 M) for 12 h. Then, the above films were rinsed several times with deionized water and immersed into a $NaBH_4$ (or AA) aqueous solution (0.01 M) for different times. Finally, the products were washed several times with deionized water and dried under a stream of N_2.

2.4 Preparation of samples for surface enhanced Raman scattering

50 μL of 4-ATP ethanol solution at different concentrations was dropped onto the surface of the GO-P4VP/Au composites. The above substrates were washed with ethanol to remove free 4-ATP molecules and then dried under a stream of N_2 for Raman examination.

2.5 Characterization

Scanning electron microscopy (SEM) images were obtained using a Hitachi SU-70 SEM system operated at 5 kV. High-resolution transmission electron microscopy (HR-TEM) images were acquired using a JEOL 2100HR electron microscope. X-ray photoelectron spectroscopy (XPS) data were recorded on an Axis Ultra Dld photoelectron spectrometer with Al Kα X-rays at an energy of 1486.6 eV. Raman spectra were recorded using a Renishaw micro Raman spectroscopy system with 633 nm laser excitation, and a CCD camera with 4 cm^{-1} resolution was employed as the detector. The spectra were obtained by focusing a 1 μm laser spot on the sample and recording for 30 s.

3. Results and discussion

3.1 Characterization of the GO-P4VP/Au composites

Fig. 1A shows that a GO film of about 800 nm thickness is formed when GO flakes are transferred onto the NH_2-terminated silicon wafer surface. After grafting the P4VP brushes *via* SIPGP, the total thickness of the as-obtained GO-P4VP film increases to 1300 nm (Fig. 1B).

Fig. 2 shows the SEM images of the relevant products when the $AuCl_4^-$ ions loaded on the GO-P4VP film were reduced using $NaBH_4$. From these images, it was found that small Au NPs are obtained in the initial stage (Fig. 2A, a). This result is in agreement with the previous report in which it was demonstrated that polymer brush-immobilized $AuCl_4^-$ could be rapidly reduced to small Au NPs using $NaBH_4$ as a reducing agent.[17] After 15 min, it was observed that the dense Au NPs became distributed uniformly on the surface of the GO-P4VP film (Fig. 2B, b). As the reaction further proceeded, the Au NPs increasingly merged together to form a compact Au film (Fig. 2C, c and D, d).

It has been reported that hierarchical Au or Ag NPs could be obtained through a nonequilibrium, kinetically controlled synthesis process.[18] Slowing down the reduction process (*i.e.* a lower reaction rate) is favourable for the formation of more complicated structures.[19] Compared to $NaBH_4$, ascorbic acid (AA), a weaker reducing agent, can provide a slow reducing rate for the nonequilibrium, kinetically controlled process of anisotropic growth.[20] Fig. 3 shows the SEM images of the as-obtained Au mesostructures using AA as a reducing agent. Initially, it is

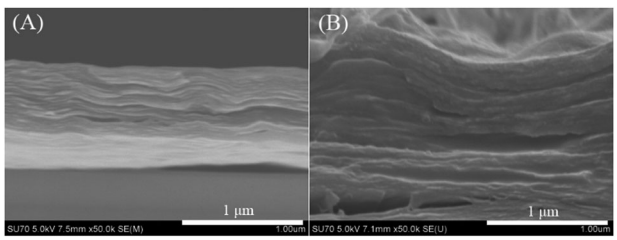

Fig. 1 Cross-sectional views of the GO film (A) and the GO-P4VP film (B).

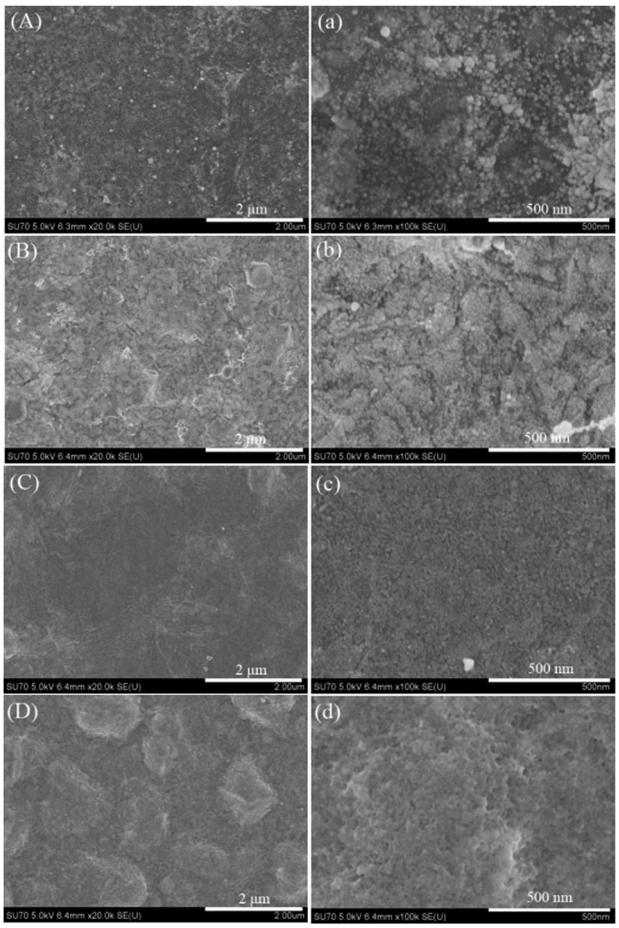

Fig. 2 SEM images of the Au nanostructures: $AuCl_4^-$ loaded on the GO-P4VP film was reduced by $NaBH_4$ for 5 min (A, a), 15 min (B, b), 30 min (C, c), and 60 min (D, d).

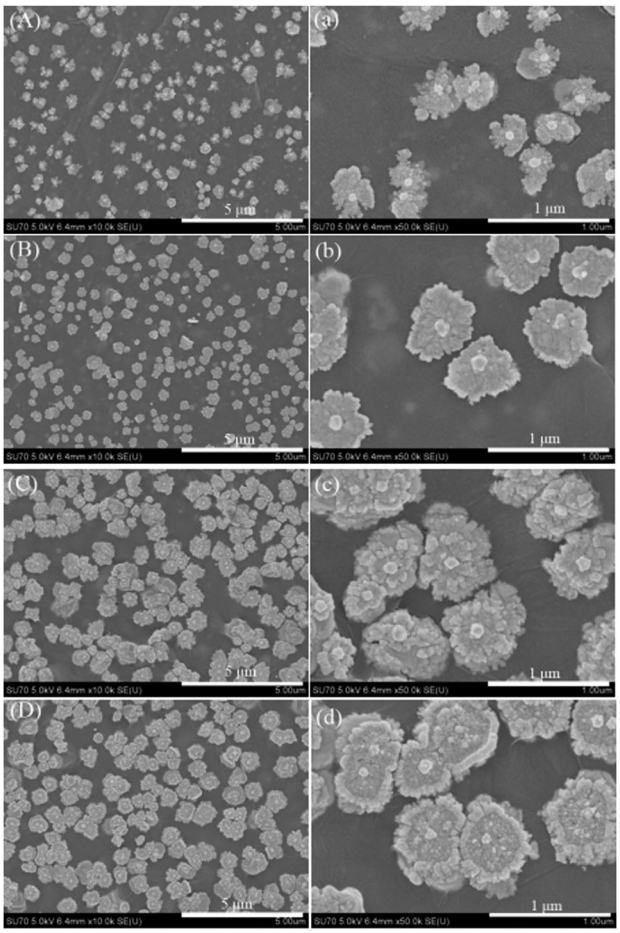

Fig. 3 SEM images of the Au mesostructures: $AuCl_4^-$ loaded on the GO-P4VP film was reduced by AA for 5 min (A, a), 15 min (B, b), 30 min (C, c), and 60 min (D, d).

found that a protrusion (spherical Au NP) surrounded by some irregular fragments forms (Fig. 3A, a). These fragments around the central protrusion grow laterally and the size of the whole mesostructure enlarges gradually (Fig. 3B, b). As the growth further proceeds, besides the size of the nanostructure continually increasing, multiple planar fragments appear on the former fragments (Fig. 3C, c). Finally, the boundary of the mesostructure keeps growing into a continuous bump (Fig. 3D, d). Interestingly, the central protrusion remains basically the same during the growth procedure.

The TEM images of a single fried egg-like Au mesostructure and its outermost boundary are shown in Fig. 4A and B, respectively. A selected-area high-resolution transmission electron microscopy (HRTEM) image is shown Fig. 4C, and the measured lattice spacing of about 0.23 nm corresponds to the (111) plane of Au.[21] A selected-area electron diffraction (SAED) pattern was obtained (Fig. 4D), indicating that the Au mesostructure is crystalline.

X-ray photoelectron spectroscopy (XPS) was conducted to elucidate the chemical composition of the as-obtained GO-P4VP/Au composites. As shown in Fig. 5A(a), the original GO film exhibits a predominant C 1s peak and an O 1s peak at *ca.* 286 eV and *ca.* 533 eV, respectively. Fig. 5B shows the high-resolution C 1s spectrum of the GO film including peaks for C═C/C–C (284.6 eV), C–O (286.5 eV), C═O (288.3 eV), and O–C═O (290.3 eV).[22] Compared with the original GO film, a new peak at *ca.* 398.5 eV attributable to the N 1s species of the imine moiety (–N═) of the pyridine rings can be observed in Fig. 5A(b) and its high-resolution spectrum is shown in Fig. 5C, indicating that the P4VP brushes had been grafted onto the GO film.[23] The XPS spectrum of the survey scan of the GO-P4VP/Au composite exhibits obvious Au 4f and Au 4d peaks in Fig. 5A(c). As shown in Fig. 5D, the Au $4f_{7/2}$ and Au $4f_{5/2}$ peaks located at *ca.* 83.6 eV and *ca.* 87.4 eV, respectively, signify that the Au element is in the zero-valent state.[24]

On the basis of the above experimental results, a hypothesis of the growth mechanism of the fried egg-like Au mesostructures is proposed. Since the reducing ability of AA is weaker than that of $NaBH_4$, a portion of $AuCl_4^-$ ions anchored on the P4VP chains is reduced to tiny Au nanocrystals along the P4VP chains. These reduced Au nanocrystals are moved toward the polymer brush surface due to a repulsive force imposed by the polymer chains and they form small Au NPs, which act as ''central sites''. As the reduction reaction continues, more Au nanocrystals

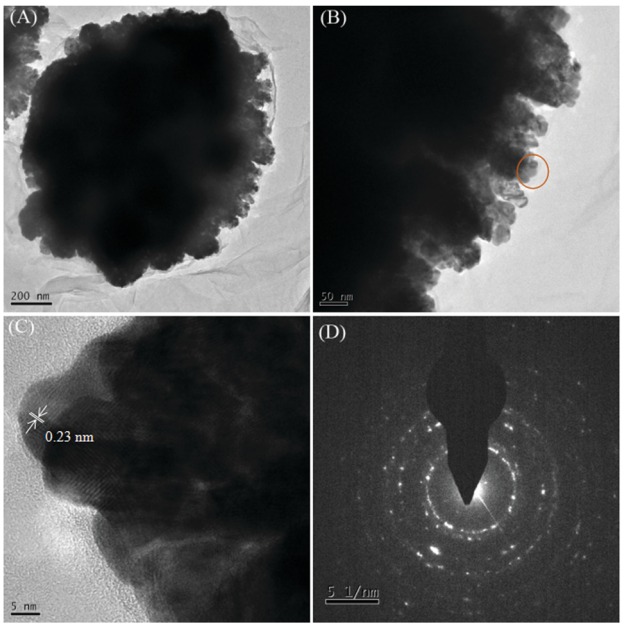

Fig. 4 (A) TEM image of a single fried egg-like Au mesostructure. (B) TEM image of the boundary of the Au mesostructure. (C) Selected-area HRTEM image. (D) SAED pattern.

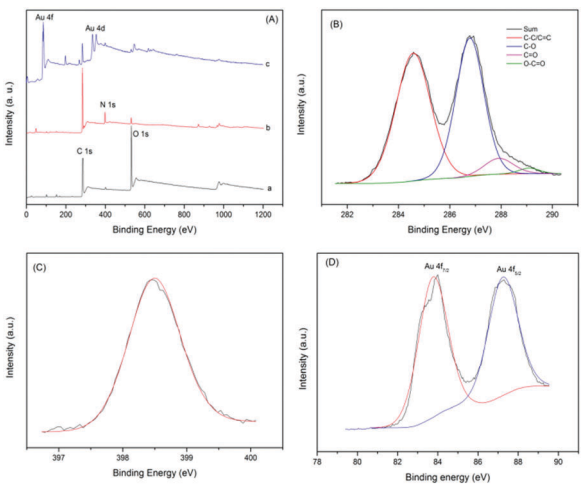

Fig. 5 (A) XPS survey spectra of the products: GO films (a), GO-P4VP films (b), and GO-P4VP/Au composites (c). (B) Curve fit of the C 1s peak of the GO film. (C) N 1s XPS spectrum of the P4VP brushes. (D) High-resolution XPS spectrum of Au 3d.

assemble around the central sites into fried egg-like mesostructures. In fact, the whole process could involve a complicated interaction between the Au NPs and polymer brushes, and efforts aimed at understanding the actual growth mechanism are underway.

3.2 The application of GO-P4VP/Au composites in SERS

The application of GO-P4VP/Au composites in SERS was investigated using 4-aminothiophenol (4-ATP) as the model analyte. The SERS spectra of 4-ATP (10^{-4} M) on the four substrates shown in Fig. 3(A–D) are shown in Fig. 6A. Compared with the

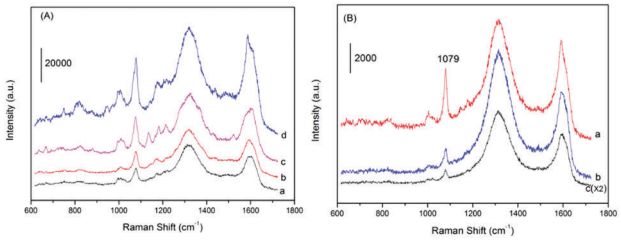

Fig. 6 (A) Raman spectra of 4-ATP (10^{-4} M) on the different Au mesostructures (as imaged in Fig. 3). (B) Raman spectra of different concentrations of 4-ATP on the Au mesostructure (as imaged in Fig. 3D): (a) 10^{-6} M, (b) 10^{-7} M, and (c) 10^{-8} M.

Raman spectra of Au nanostructures shown in Fig. 2 and Fig. S1 (ESI†), the fried egg-like Au mesostructures exhibit more SERS enhancement ability. In addition, as can be seen from Fig. 6A, among the four substrates, the 60 min sample (as imaged in Fig. 3D) exhibits the best SERS enhancement. This result may be attributed to its hierarchical architectures: the irregular polyhedron morphology, nanoscale junctions and nanoscale roughness can provide more "hot spots",[25–32] thus giving a strong SERS signal. The enhancement factor (EF) of 4-ATP on the fried egg-like Au mesostructures was calculated to be about 3.78×10^4 (the detailed calculation can be seen in the ESI†). This value is equal or close to that reported by other research groups.[33,34] The limit of SERS *versus* 4-ATP concentration was evaluated using the above substrate and lower concentrations of the 4-ATP solutions from 10^{-6} to 10^{-8} M were used here. As shown in Fig. 6B, when the 4-ATP concentration decreases to 10^{-8} M, the feature peak at 1079 cm^{-1} can still be easily identified. The results imply that the as-fabricated fried egg-like Au mesostructures can be used as SERS substrates with high sensitivity for the trace detection of analytes.

4. Conclusions

In summary, we have demonstrated that Au structures with different morphologies can be prepared through the choice of reducing agents to reduce $HAuCl_4$-loaded GO-P4VP film. Thin gold films composed of small Au NPs were obtained through the reduction of $HAuCl_4$-loaded GO-P4VP film using $NaBH_4$ and fried egg-like Au mesostructures were obtained using AA as a reducing agent. The as-obtained fried egg-like Au mesostructures were identified as an efficient SERS substrate for the trace detection of 4-ATP molecules.

Conflicts of interest

There are no conflicts to declare.

Acknowledgements

This work was supported by the Natural Science Foundation of Zhejiang (LY18E030003) and K. C. Wong Magna Fund in Ningbo University.

Notes and references

1 K. Kneipp, H. Kneipp, I. Itzkan, R. R. Dasari and M. S. Feld, *Chem. Rev.*, 1999, **99**, 2957–2976.
2 J. X. Feng, S. Y. Du, S. Lebedkin, Z. Y. Li, R. Kruk, M. Kppes and H. Hahn, *Nano Lett.*, 2010, **10**, 5006–5013.
3 C. Tan, X. Huang and H. Zhang, *Mater. Today*, 2013, **16**, 29–36.
4 L. Kang, J. Chu, H. Zhao, P. Xu and M. Sun, *J. Mater. Chem. C*, 2015, **3**, 9024–9037.
5 N. Zhang, L. Tong and J. Zhang, *Chem. Mater.*, 2016, **28**, 6426–6435.
6 X. Ling, L. Xie, Y. Fang, H. Xu, H. Zhang, J. Kong, M. S. Dresselhaus, J. Zhang and Z. Liu, *Nano Lett.*, 2009, **10**, 553–561.
7 X. Li, Y. Zhang, Y. Wu, Y. Duan, X. Luan, Q. Zhang and Q. An, *ACS Appl. Mater. Interfaces*, 2015, **7**, 19353–19361.
8 L. Guo, Q. Liu, G. Li, J. Shi, J. Liu, T. Wang and G. Jiang, *Nanoscale*, 2012, **4**, 5864–5867.
9 M. Steenackers, A. M. Gigler, N. Zhang, F. Deubel, M. Seifer, L. H. Hess, C. H. Y. X. Lim, K. P. Loh, J. A. Garrido, R. Jordan, M. Stutzmann and I. D. Sharp, *J. Am. Chem. Soc.*, 2011, **133**, 10490–10498.
10 R. Contreras-Caceres, C. Dawson, P. Formanek, D. Fischer, F. Simon, A. Janke, P. Uhlmann and M. Stamm, *Chem. Mater.*, 2013, **25**, 158–169.
11 S. Gupta, M. Agrawal, M. Conrad, N. A. Hutter, P. Olk, F. Simon, L. M. Eng, M. Stamm and R. Jordan, *Adv. Funct. Mater.*, 2010, **20**, 1756–1761.
12 D. Han, P. Xiao, J. Gu, J. Chen, Z. Cai, J. Zhang, W. Wang and T. Chen, *RSC Adv.*, 2014, **4**, 22759–22762.
13 G. Xing, K. Wang, P. Li, W. Wang and T. Chen, *Nanotechnology*, 2018, **29**, 115503.
14 G. Xing, W. Wang, K. Wang, P. Li and T. Chen, *Chem. – Eur. J.*, 2017, **23**, 17549–17555.
15 W. S. Hummers and R. E. Offeman, *J. Am. Chem. Soc.*, 1958, **80**, 1339.
16 P. Xiao, S. Y. Du, T. Zhang, N. X. Qiu, J. W. Zhang, Y. J. Huang, C. J. Wan, R. Jordan, Q. Huang, Z. P. Liu and T. Chen, *Adv. Mater. Interfaces*, 2017, **4**, 1600867.
17 O. Azzaroni, A. A. Brown, N. Cheng, A. Wei, A. M. Jonas and W. T. Huck, *J. Mater. Chem.*, 2007, **17**, 3433–3439.
18 B. Viswanath, P. Kundu, A. Halder and N. Ravishanka, *J. Phys. Chem. C*, 2009, **113**, 16866–16883.
19 Y. Xia, Y. Xiong, B. Lim and S. E. Skrabalak, *Angew. Chem., Int. Ed.*, 2009, **48**, 60–103.
20 D. P. Huang, Y. Y. Qi, X. T. Bai, L. J. Shi, H. Jia, D. J. Zhang and L. Q. Zheng, *ACS Appl. Mater. Interfaces*, 2012, **4**, 4665–4671.
21 Z. Liu, F. L. Zhang, Z. B. Yang, H. J. You, C. F. Tian, Z. Y. Li and J. X. Fang, *J. Mater. Chem. C*, 2013, **1**, 5567–5576.
22 J. He, P. Xiao, J. W. Zhang, Z. Z. Liu, W. Q. Wang, L. T. Qu, Q. Ouyang, X. F. Wang, Y. S. Chen and T. Chen, *Adv. Mater. Interfaces*, 2016, **3**, 1600169.
23 J. L. Liu, L. F. Zhang, S. P. Shi, S. Chen, N. C. Zhou, Z. B. Zhang, Z. P. Cheng and X. L. Zhu, *Langmuir*, 2010, **26**, 14806–14813.
24 D. Paripovic and H. A. Klok, *ACS Appl. Mater. Interfaces*, 2011, **3**, 910–917.
25 H. Wang and N. J. Halas, *Adv. Mater.*, 2008, **20**, 820–825.
26 Y. J. Huang, A. Dandapa and D.-H. Kim, *Nanoscale*, 2014, **6**, 6478–6481.
27 J. Theiss, P. Pavaskar, P. M. Echternach, R. E. Muller and S. B. Cronin, *Nano Lett.*, 2010, **10**, 2749–2754.
28 Q. F. Zhang, N. Large and H. Wang, *ACS Appl. Mater. Interfaces*, 2014, **6**, 17255–17267.
29 Y. J. Huang, A. Dandapat and D.-H. Kim, *Nanoscale*, 2014, **6**, 6478–6481.
30 Y. J. Huang, A. R. Ferhan, H.-J. Cho, H. Lee and D.-H. Kim, *ACS Appl. Mater. Interfaces*, 2015, **7**, 17582–17586.
31 J. M. Chen, Y. J. Huang, P. Kannan, L. Zhang, Z. Y. Lin, J. W. Zhang, T. Chen and L. H. Guo., *Anal. Chem.*, 2016, **88**, 2149–2155.
32 X. F. Lu, Y. J. Huang, B. Q. Liu, L. Zhang, L. P. Song, J. W. Zhang, A. F. Zhang and T. Chen, *Chem. Mater.*, 2018, **30**, 1989–1997.
33 Y. L. Wang, S. J. Guo, H. J. Chen and E. K. Wang, *J. Colloid Interface Sci.*, 2008, **318**, 82–87.
34 Z. Yi, J. S. Luo, X. L. Tan, Y. Yi, W. T. Yao, X. L. Kang, X. Ye, W. K. Zhu, T. Duan, Y. G. Yi and Y. J. Tang, *Sci. Rep.*, 2015, **5**, 16137.